Received: 1 August 2023 | Revised: 15 November 2023 | Accepted: 13 December 2023

DOI: 10.1002/eqe.4074

RESEARCH ARTICLE

WILEY

Displacement-based design procedures for rigid block isolation

Giacomo Destro Bisol[1] | **Matthew J. DeJong**[2] | **Domenico Liberatore**[3] | **Luigi Sorrentino**[1]

[1]Department of Structural and Geotechnical Engineering, University of Rome La Sapienza, Rome, Italy

[2]Department of Civil and Environmental Engineering, University of California, Berkeley, Berkeley, California, USA

[3]Department of History, Representation and Restoration of Architecture, University of Rome La Sapienza, Rome, Italy

Correspondence
Luigi Sorrentino, Department of Structural and Geotechnical Engineering, University of Rome La Sapienza, Via Antonio Gramsci 53, Rome 00197, Italy.
Email: luigi.sorrentino@uniroma1.it

Funding information
MONALISA; Lazio Regional Government; Italian Ministry of University and Research, Grant/Award Number: 305-2020-35576

Abstract

When subjected to earthquakes, many objects or structural elements behave like rocking rigid blocks. Computer servers, medical shelves, art objects, statues, and electrical transformers are frequently included in this category. Protection of these objects is an important task, considering that their value could be inestimable or their operation crucial during earthquakes; base isolation technology has been proven to be a viable option for this purpose. Initially, the dynamic model of a rocking rigid block placed on a base isolation device is reviewed. Then, two equivalent-static displacement-based procedures for designing the isolators for these types of objects are proposed, and the main steps are illustrated. The first procedure aims to determine isolator characteristics to prevent the initiation of rocking motion during the code-level earthquake event. The second procedure is aimed at designing isolators that allow a specified maximum rotation of the block during seismic events. The proposed procedures are validated by means of time-history analyses for a suite of spectrum-compatible accelerograms. The first displacement-based procedure appears particularly suitable for objects of small to medium size. The validation of the second procedure demonstrates that the equal displacement rule can be applied for this kind of systems, despite their softening. The results also indicate that the approach is particularly effective for medium to large structures/objects, if small oscillations are acceptable. The controlled rocking procedure offers a significant advantage by allowing for a reduction in the maximum displacement and period of the isolator, compared to situations where rocking motion must be prevented entirely.

KEYWORDS

controlled rocking, displacement-based design procedure, overturning stability of statues and art objects, rocking prevention, rocking-body dynamics, seismic isolation of non-structural elements

1 | INTRODUCTION

A number of valuable objects and structural elements, such as computer servers, art pieces, electrical transformers, portions of masonry buildings, and bridge piers, exhibit rocking behavior during earthquakes. The dynamics of rigid blocks have long been a subject of interest in the field of structural engineering. In particular, the rocking behavior of rigid blocks has significant implications in the seismic assessment of slender structures/objects. The literature contains a large number of analytical studies on the dynamics of rigid blocks, starting with the study on a single block presented by Housner.[1] Further studies[2] highlighted the complexity of the rigid block response to real earthquakes, pointing out the high sensitivity to geometry and ground motion of this type of system. Recently, rigid block modeling has received attention for the assessment of the seismic vulnerability[3–5] of masonry structures[6–9] and nonstructural elements.[10–15] Further, a variety of experimental tests have been conducted to investigate the response of rocking objects during earthquakes, such as art objects,[16,17] and hospital cabinets.[18,19]

Base isolation technology can present a practical solution for the seismic protection of rocking objects. The subject of base isolation technology used for seismic protection in general has received extensive attention in recent decades,[20–22] and numerous investigations into response control and seismic isolation were conducted. Remarkable progress has been achieved in advancing these technologies,[23,24] which fall in the well-known "passive control" category of structural control.

Seismic isolation technology used to protect rocking rigid objects received attention, mainly to preserve nonstructural elements such as computer servers or art objects.[25–27] These studies generally confirmed the efficiency of the seismic isolation technology.[28–30] Vassiliou and Makris[31] explored the response of different base isolation technologies for rocking rigid blocks subjected to earthquakes. Furthermore, it has been observed that increasing the size of the block can also contribute to enhancing the performance of the base isolation.[32] Recently, the emphasis has shifted to the investigation of novel constitutive laws for the isolation system[33] or innovative protection technologies.[34–38] In addition to many theoretical studies, base isolation applications have also been documented, mainly oriented towards the protection of art objects. Among them are the Hermes of Praxiteles at the archaeological museum of Olympia, Greece, the Gates of Hell by Rodin at the national museum of Western Art in Tokyo, Japan, and some movable works of art at the J. Paul Getty museum in Los Angeles, USA.[25] Friction pendulum devices were used in the first two cases and a device formed by springs in the third. An application of vibration protection was also carried out in Italy for the Rondanini Pietà in the Castello Sforzesco in Milan,[39] however the most relevant example is that of the Riace Bronzes, for which a novel marble antiseismic basement was used.[35] Additional applications have focused on using floor isolation[40,41] to protect crucial nonstructural objects (i.e., computers servers and medical equipment). This technology proved to be effective because it allows the protection of specific rooms that contain sensitive objects as opposed to isolating the entire building. Finally, other examples can be found for the protection of large electrical transformers,[42,43] equipment in nuclear power plants[44] and nonstructural elements in medical facilities.[45,46]

Further, numerous studies were conducted in the last decades on the displacement-based procedure to design and assess structures subjected to earthquakes.[47,48] The success of this procedure is due to its simplicity and efficacy, while accounting for the nonlinear response of the investigated system; researchers developed several displacement-based methods to design and assess different structures, that is, frame structures and bridges.[49] Further, many studies were conducted to develop displacement-based procedures to design different seismic protection strategies, such as base isolation technology.[50–52] Moreover, attempts were made in order to define simplified design/assessment procedure for rocking rigid blocks subjected to earthquake[53] assuming the rigid block as a system with one degree of freedom (DOF). The use of response spectrum for rocking blocks idealized as a single DOF system was proven not be generally valid by Makris and Konstantinidis.[54] For this reason, the sensitivity of rigid block responses to seismic inputs was extensively investigated. In particular, the simplification of seismic inputs, involving resonance conditions via single or multiple impulses,[55–57] proved to be particularly effective for replacing response-spectrum analysis and highlighting some features of the dynamic behavior of this oscillator. Recently, simplified analysis procedures have been developed for rocking systems[58] and for systems exhibiting negative stiffness.[59] However, there is currently no procedure available for designing base isolation associated with rocking.

Despite the conclusions of Makris and Konstantinidis,[54] simplified design procedures, based on the response spectrum analysis, to design isolation systems for rigid rocking blocks are proposed here. The assumptions that motivate this work as well as the reasons why the equivalent elastic system is acceptable for this system and not generally applicable to the fixed-base rigid block are: (a) the presence of an elastic-viscous system beneath the rigid block significantly influences the

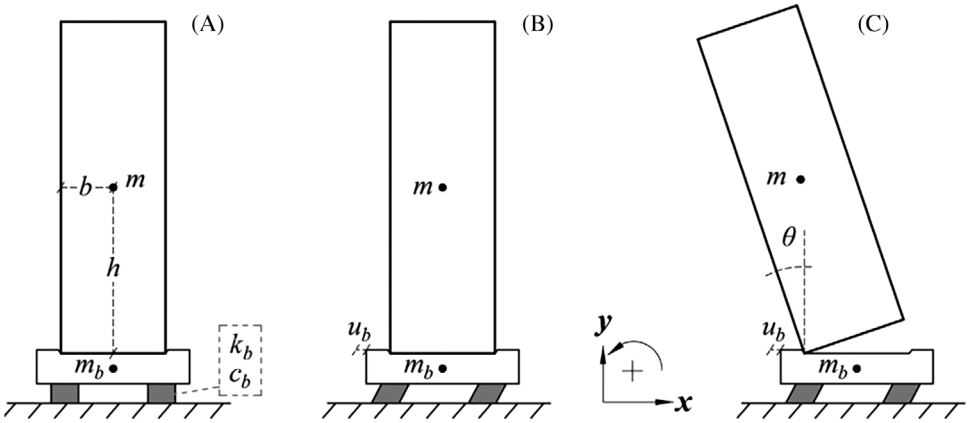

FIGURE 1 Configurations of the seismically isolated rigid block system: (A) system at rest (B) pure translation; (C) translation plus rocking.

overall behavior; (b) in this study the displacement-based design approach is used, as opposed to the force-based approach proposed by Priestley et al.[53]; (c) the assumption of small rotations of the block and large displacements of the isolator results in the system being primarily governed by a linear elastic oscillator that closely aligns with the response spectrum; (d) in the proposed procedures rocking rotations are zero or small, hence far away from the unstable equilibrium position, $\theta = \alpha$[60] close to which the high sensitivity of the rocking block to small variations of the system parameters was extensively documented.[2,54]

Considering the previous assumptions, two displacement-based procedures to design isolation systems for rigid rocking blocks are proposed in this paper: (a) the prevented rocking displacement-based design (PRDBD) procedure, which is aimed at designing the isolator to prevent initiation of rocking motion during the design earthquake; (b) the controlled rocking displacement-based design (CRDBD) procedure, which is aimed at designing base isolation devices for rocking blocks, in order to allow a specified maximum rotation during the code earthquake. The proposed procedures are then validated by examining the dynamic response of the system to a suite of spectrum-compatible accelerograms. Finally, some practical examples using the proposed procedures are presented, and an assessment/protection procedure for slender rocking objects is depicted.

2 | REVIEW OF THE ISOLATED RIGID ROCKING BLOCK MODEL

The analytical model of a rigid block placed on a base isolation device[28,29,31] is summarized in this section. The system consists of a rocking block with half height h, half width b, and mass m placed on a linear isolation device characterized by mass m_b, stiffness k_b, and viscous damping c_b (Figure 1A). A large frictional force that prevents sliding is assumed, hence the block is limited to rock only about its corners, and instantaneous impacts are considered. The motion of the system is described by two configurations; (a) the block and the isolator translate horizontally together (Figure 1B); (b) the isolator is moving while the block is rocking (Figure 1C).

When the motion of the system is characterized by pure translation, the system is described by one DOF only: the horizontal translation of the linear isolator u_b. The equation of motion in this case is simply:

$$m_t \ddot{u}_b = -u_b k_b - \dot{u}_b c_b - \ddot{x}_g m_t, \tag{1}$$

where $m_t = m + m_b$ is the total mass of the system (sum of block mass and isolator mass), $\ddot{x}_g$ is the horizontal component of the seismic ground acceleration, and the dot superscript indicates derivative with respect to time.

If the sum of the horizontal component of ground motion and the base isolation acceleration, $(\ddot{x}_g + \ddot{u}_b)$, exceeds the threshold (or uplift) acceleration, the block starts to rock (Figure 1C). In this configuration, the motion of the system is characterized by two DOFs: the horizontal displacement of the isolator and the rotation of the rigid block, θ. The equations

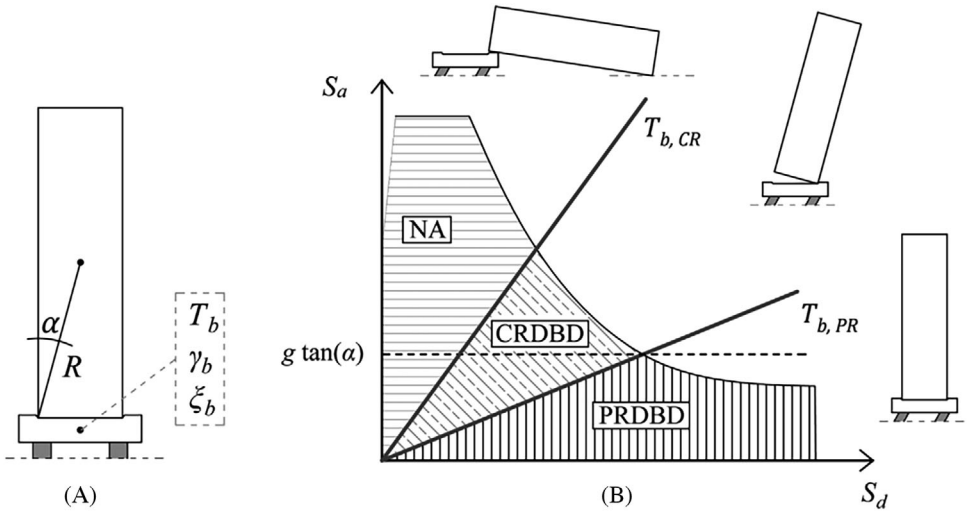

FIGURE 2 (A) Geometrical and mechanical properties of the isolated rigid rocking block system, (B) Displacement-based procedures depicted in the ADRS plane. ADRS, acceleration-displacement response spectrum.

of motion for this configuration[28,29,31] can be expressed in matrix form as:

$$\begin{bmatrix} I_G + \left(b^2 + h^2\right) & m & -m\ (h\cos(\theta) + S_\theta\, b\sin(\theta)) \\ sym & & m_t \end{bmatrix} \cdot \begin{Bmatrix} \ddot{\theta} \\ \ddot{u}_b \end{Bmatrix}$$

$$= \begin{Bmatrix} m\,\ddot{x}_g\,(h\cos(\theta) + S_\theta\, b\sin(\theta)) + m\,g\ (h\sin(\theta) - S_\theta\, b\cos(\theta)) \\ m\,(S_\theta\, b\cos(\theta) - h\sin(\theta))\,\dot{\theta}^2 - u_b\,k_b - \dot{u}_b\,c_b - \ddot{x}_g\,m_t \end{Bmatrix}, \tag{2}$$

where I_G is the mass moment of inertia of the block with respect to its centroid G, g is the gravitational acceleration and S_θ is the signum function:

$$S_\theta = 1 \text{ if } \theta > 0 \text{ or } S_\theta = -1 \text{ if } \theta < 0;$$

Further, in the configuration where the rocking motion is initiated, impacts between the block and the isolator may occur. The calculation of the postimpact velocities of the isolated-base case differs from that of the fixed-base one because the base isolator also undergoes a change in velocity.[31] Therefore, it is necessary to evaluate the postimpact velocities for both the isolator and the rigid block. In this study, the procedure proposed by Vassiliou and Makris[31] is used to calculate the coefficients to be applied to preimpact velocities, usually called coefficients of restitution. From now, to reduce the dimensions of the problem, the characteristics of the isolator are described using the period, T_b, the mass ratio, γ_b, and the damping ratio, ξ_b (Figure 2A), as:

$$T_b = 2\pi\sqrt{m_t/k_b};\ \gamma_b = \frac{m}{m_t};\ \xi_b = \frac{c_b}{2\omega_b m_t}, \tag{3}$$

where $\omega_b = \sqrt{k_b/m_t}$ is circular frequency of the isolator.

Similarly, the block is assumed rectangular in shape and is thus described by its slenderness angle α (the more slender, the smaller the value of α), size parameter R (Figure 2A), and the frequency parameter p as follows:

$$\alpha = \tan^{-1}\left(\frac{b}{h}\right);\ R = \sqrt{b^2 + h^2};\ p = \sqrt{3\,g/4R} \tag{4}$$

3 | DISPLACEMENT-BASED DESIGN PROCEDURES FOR ISOLATED ROCKING STRUCTURES

Two simplified procedures to design isolation systems for rocking rigid blocks are described in this section: (a) Prevented rocking displacement-based design (PRDBD); (b) Controlled rocking displacement-based design (CRDBD). The former aims to design a base isolation device in order to prevent the initiation of rocking motion of the rigid block, while in the latter the base isolation is designed to control the maximum rotation of the block.

The two procedures can be depicted using the acceleration-displacement response spectrum (ADRS), which allows a prompt understanding of the problem. In Figure 2B, a free-field (or ground) response spectrum is used, but the proposed procedure can be easily extended to floor spectra.[61,62] Two distinct periods of base isolation can be found in the spectrum (Figure 2B): (a) $T_{b,PR}$, that corresponds to the threshold acceleration initiating rocking motion, $g\tan(\alpha)$; (b) $T_{b,CR}$, that is the period for which the block, during the code earthquake, undergoes a specific absolute maximum rotation. These two periods define three regions in the ADRS plane. The first area lies below $T_{b,PR}$ and it includes all those periods for which the base isolation prevents initiation of rocking motion under the design earthquake. The boundaries of this region depend on the seismic demand, on the damping of the isolator and on the slenderness of the block (but not on its size).

The region that lies between $T_{b,PR}$ and $T_{b,CR}$ includes all those periods of the base isolation for which the rocking motion is triggered, and the absolute maximum rotation that the rigid block experiences should not exceed the capacity of the block. The boundaries of this region are determined by the seismic demand, the damping of the isolator, and the slenderness of the block (as is the case for the region below $T_{b,PR}$), but also by the size of the block (which is from now described using the frequency parameter p). It is important to note that, due to the extreme nonlinearity of rocking motion, the rotations of the rigid block during the code earthquake may exceed the assumed capacity of the block (or even overturn it) also for isolators with period longer than $T_{b,CR}$. Similarly, the region above $T_{b,CR}$ includes all those periods of the base isolation for which the rocking motion is triggered, and large nonacceptable (NA) rotations are expected. In this area overturning or rotations larger than the assumed maximum capacity of the block may occur, therefore the procedures are no longer applicable. Also in this area, due to the nonlinearity of the rocking response, the block placed on an isolator with period longer than $T_{b,CR}$ might not overturn or exhibits rotation smaller than those expected.

3.1 | Steps of the prevented rocking displacement-based design procedure

The PRDBD procedure has the goal of designing the base isolation system to prevent rotations of the rigid block. This procedure (Figure 3) is particularly suitable for small to medium size objects (more vulnerable to earthquakes), whose values may be inestimable (such as art objects), or whose operation is essential during earthquakes (such as medical equipment). The slenderness angle of the block is assumed to be known, and consequently also the uplift acceleration. In this procedure, the isolated block assembly can be simplified to a single DOF system with equivalent mass coincident with the total mass m_t of the system, equivalent stiffness coincident with the stiffness of the isolator k_b, and equivalent damping ratio coincident with the damping ratio ξ_b of the isolator. The block is expected not to rock when subjected to the design earthquake filtered by the isolator, hence the stiffness of the block, k_s, can be assumed infinite. Rocking motion can be avoided by imposing that the maximum spectral acceleration of the single DOF system (Figure 3B) remains lower than the minimum uplift acceleration. The design of the isolator partially follows the procedure of the displacement-based design for single DOF systems, with the difference that the damping is concentrated only in the base isolation device and the maximum spectral acceleration is limited to the uplift acceleration.

In order to design the seismic protection device for slender rigid blocks the PRDBD procedure, schematically depicted using the flowchart in Figure 4A, can be applied following these steps:

1) Identify the structural dimensions and define the characteristics of the equivalent single DOF system (Figure 3A and B).
2) Define the target displacement d_t and the uplift acceleration of the block $g\tan(\alpha)$ (Figure 3C). The former is related to design requirements (and to the limits of the commercial isolators), while the latter depends only on the slenderness angle of the rigid block.

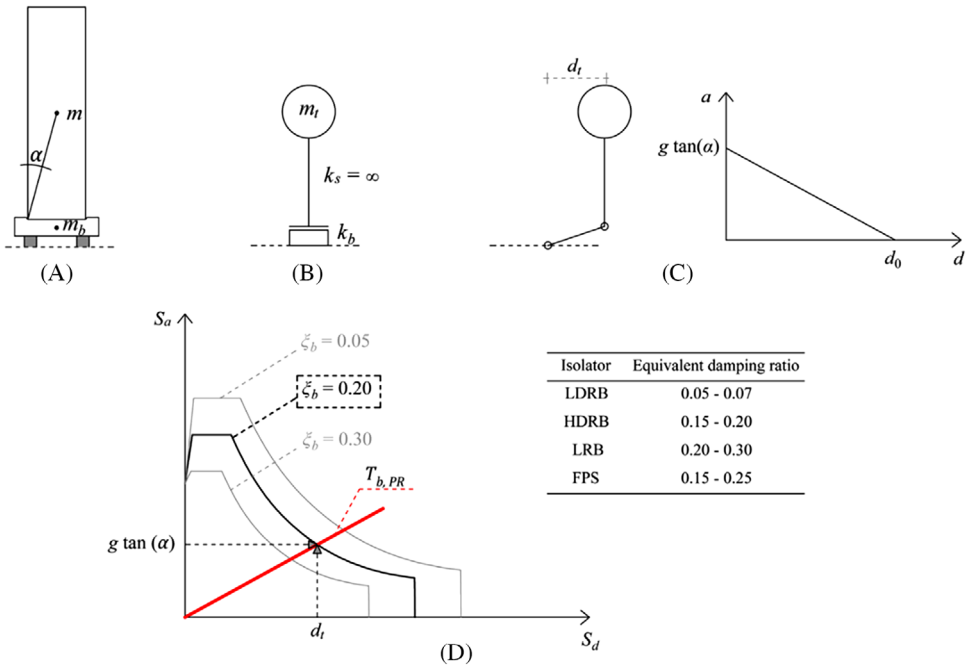

Isolator	Equivalent damping ratio
LDRB	0.05 - 0.07
HDRB	0.15 - 0.20
LRB	0.20 - 0.30
FPS	0.15 - 0.25

FIGURE 3 PRDBD procedure: (A) Properties of the system; (B) Equivalent SDOF system, (C) Displacement profile of the system and acceleration-displacement curve of the nonisolated block; (D) Demand spectrum for different damping ratios and definition of the target damping. FPS, friction pendulum system; HDRB, high damping rubber bearing; LDRB, low damping rubber bearing; LRB, lead rubber bearing; PRDBD, prevented rocking displacement-based design.

3) Define the spectral demand on the ADRS plane and calculate the period $T_{b,PR}$ of the isolator for which rocking motion is prevented as:

$$T_{b,PR} = 2\pi\sqrt{\frac{d_t}{g\tan(\alpha)}} \tag{5}$$

4) Select the target damping necessary to avoid rocking motion (Figure 3D). If necessary, the seismic demand must be properly scaled based on the equivalent damping ratio of the isolator.[63]
5) Design isolator: once the target damping is determined (Figure 3D) and the period $T_{b,PR}$ obtained, it is possible to define all the mechanical properties of the isolation device.

3.2 | Steps of the controlled rocking displacement-based design procedure

The second procedure (CRDBD) has the goal of designing the base isolation system in order to allow a controlled rocking motion of the rigid block under the code-level earthquake. This approach is suitable for medium to large size blocks, and for those for which small oscillations are acceptable. The main advantage of this procedure is that the maximum displacement of the isolator, can be reduced compared to the PRDBD method, although rocking motion is triggered with all the consequences this may imply (e.g., impacts). This method uses the rotational capacity of the block to increase the overall performance of the system. For the reasons already presented in the Introduction, the procedure is based on the assumption that the displacement response of the isolated rocking rigid block system matches that of a linear system, characterized by the period and damping of the isolator. Furthermore, the CRDBD procedure can be considered as a viable alternative to connecting the block directly to the isolator, in order to avoid excessive stress on the block caused by bolts, pins, or other anchoring systems that may lead to large (incompatible) stresses on the block. The CRDBD method is depicted as a flowchart in Figure 4B, and consists of the following steps:

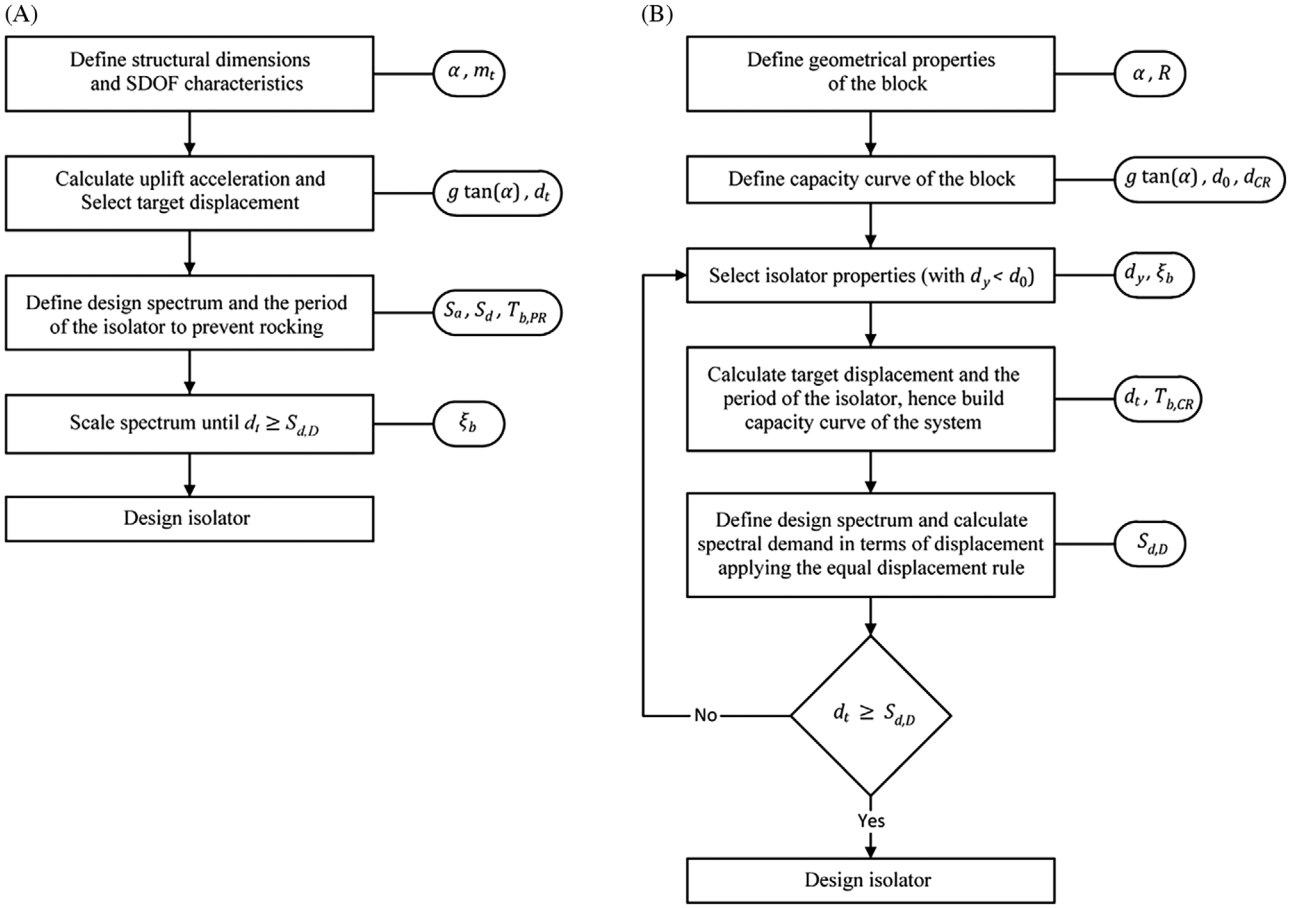

FIGURE 4 Flowcharts of: (A) PRDBD procedure; (B) CRDBD procedure. CRDBD, controlled rocking displacement-based design; PRDBD, prevented rocking displacement-based design.

1) Identify the geometrical parameters of the block, that is, α and R.
2) Define the capacity of the rigid block in terms of uplift acceleration ($g\tan(\alpha)$) and limit displacement (d_{CR}). For example, as recommended by the commentary to the Italian building code[64] for masonry structural elements, the displacement capacity of the rocking rigid block may be assumed to be 40% of the block ultimate displacement d_0 (Figure 3C).
3) Select isolator properties to define the yield displacement d_y (displacement of the isolator at the uplift acceleration) and the damping ratio ξ_b. Similarly, to the PRDBD procedure, these values are determined by the design requirements and the limits of commercial isolators.
4) Calculate the period of the isolator, $T_{b,CR}$ and the target displacement, d_t, as shown in Equation (6). Finally, build the capacity curve of the system (Figure 5A) assuming a uniform load profile.

$$T_{b,CR} = 2\pi\sqrt{\frac{d_y}{g\tan(\alpha)}};\ d_t = d_{CR} + d_{b,CR} \text{ where } d_{b,CR} = a(d_{CR})\frac{T_{b,CR}^2}{4\pi^2}, \tag{6}$$

where $d_{b,CR}$ and $a(d_{CR})$ are respectively the displacement of the isolator and the static acceleration of the block at the instant where the block reaches the assumed rotational capacity d_{CR}.

In the second branch of the capacity curve, as the displacement of the block increases, the resisting force of the system decreases. Consequently, as the rotation of the block increases, the linear isolator tends to return to its rest position. When the block reaches its maximum displacement capacity, d_0, the resisting force becomes zero, and the isolator returns to its initial position. Considering this behavior, different scenarios may arise. When the maximum capacity of the block, d_0, is smaller than the displacement of the isolator, d_y, the second

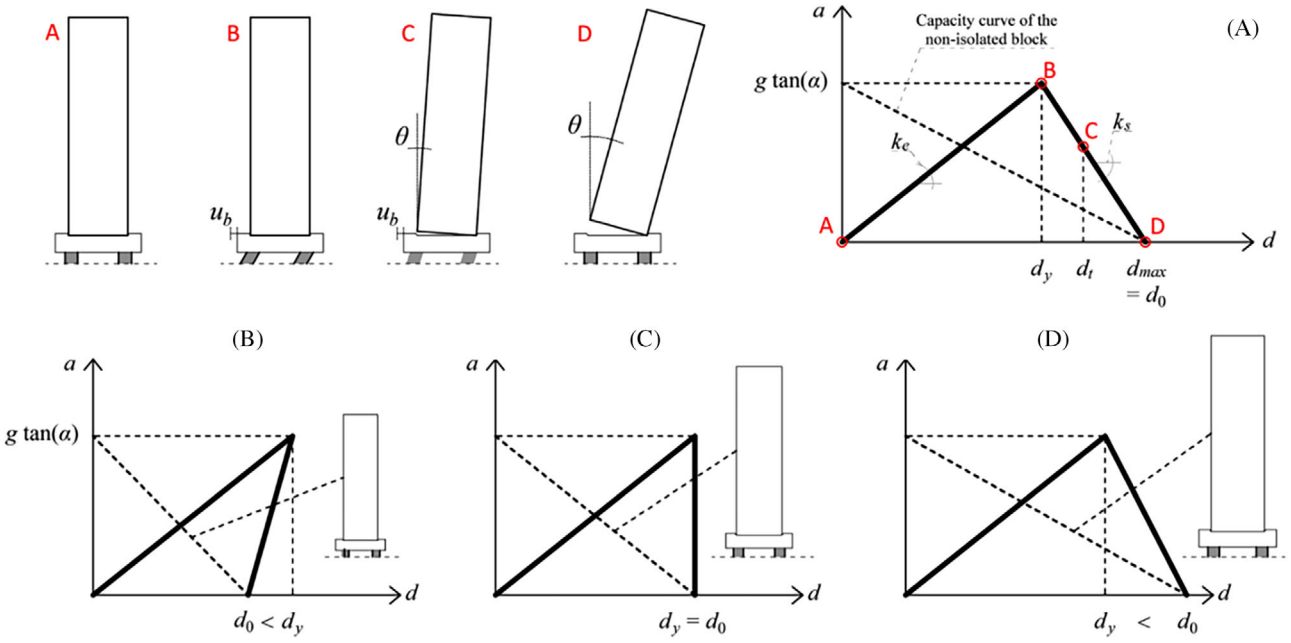

FIGURE 5 Acceleration-displacement curve for the isolated rocking rigid block system. (A) Definition of the curve. Particular cases of the capacity curve for a system with: (B) $d_y > d_0$; (C) $d_y = d_0$; (D) $d_y < d_0$.

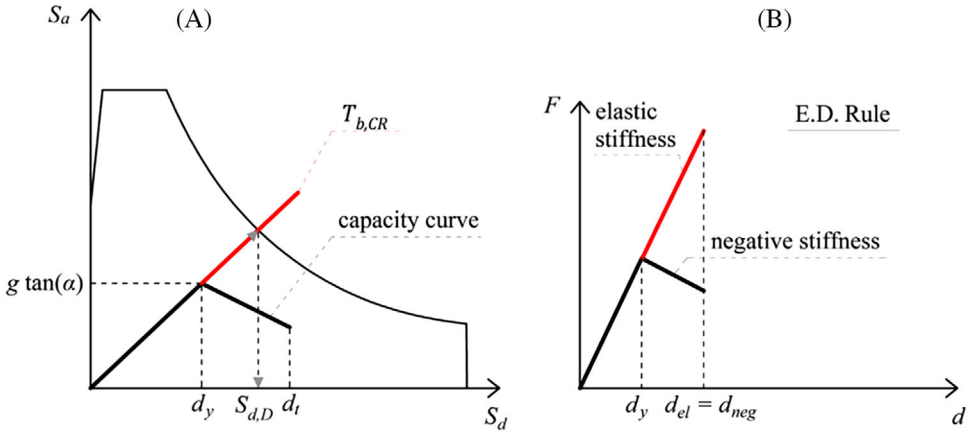

FIGURE 6 CRDBD: (A) procedure to evaluate the spectral displacement demand; (B) equal displacement rule for a system exhibiting negative stiffness. CRDBD, controlled rocking displacement-based design.

branch of the capacity curve is characterized by a snapback behavior (Figure 5B). In this case, rocking cannot be relied on as a consistent behavior in design; hence, controlled rocking is no longer an acceptable strategy for systems exhibiting snapback behavior. If possible, a stiffer isolator should be used; alternatively, the PRDBD procedure should be pursued. Additionally, when $d_y = d_0$ (Figure 5C), the response of the system transitions from an unstable (Figure 5B) to a stable configuration, thus when $d_y < d_0$ (Figure 5D) the CRDBD procedure can be applied.

5) Calculate the seismic demand in terms of displacement (Figure 6A), $S_{d,D}$, applying the equal displacement rule (Figure 6B). The displacement demand can be obtained as a function of the elastic stiffness k_e, hence from the period $T_{b,CR}$.
6) Check that the spectral demand, $S_{d,D}$, is smaller than the target displacement d_t. If the previous control is satisfied, design the mechanical properties of the isolator. If the control is not satisfied, repeat Step 3 after selecting a different

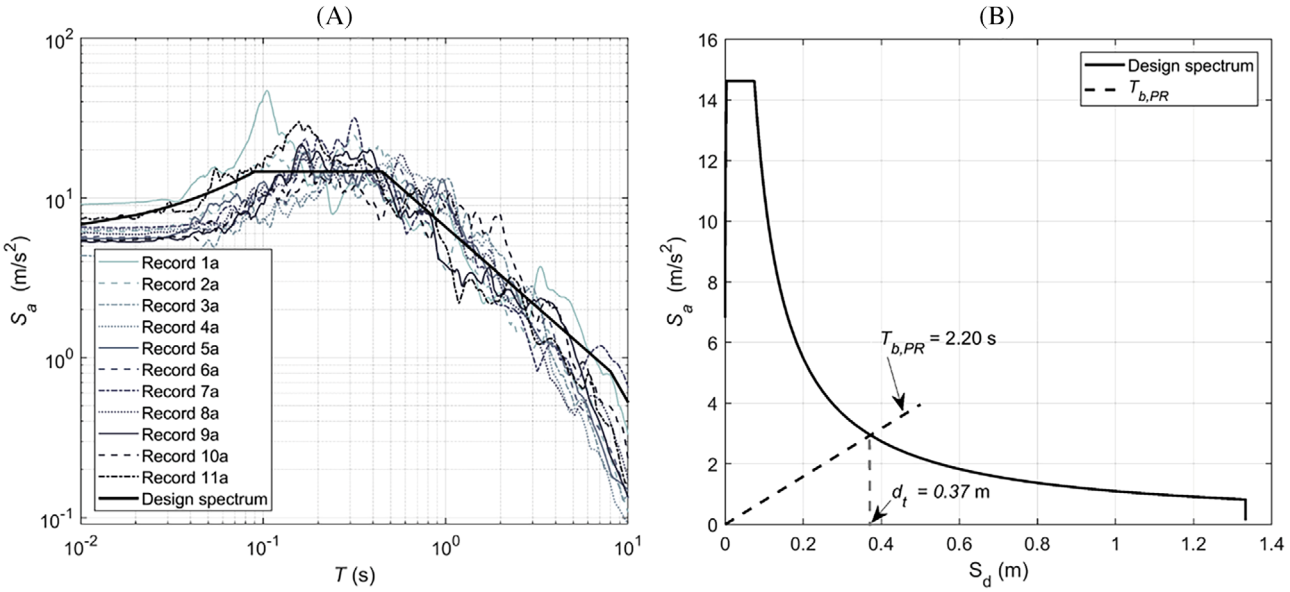

FIGURE 7 (A) Elastic response spectra of records compatible with the code seismicity of the Getty Villa, California, USA, with reference to Table A1; (B) Design spectrum and period of the isolator $T_{b,PR}$ (used in the validation study) plotted in the ADRS plane. ADRS, acceleration-displacement response spectrum.

isolator. As in the previous case, the procedure can be modified, for example, to determine the necessary damping once the target displacement is known.

Similarly to the PRDBD procedure, the proposed design procedure necessitates to scale the seismic demand according to the equivalent damping ratio of the isolator. To this purpose many procedures are present in the literature,[65] and the accuracy of the displacement-based methods strongly depends on which relation is used.[50]

4 | VALIDATION OF THE DISPLACEMENT-BASED DESIGN PROCEDURES

To validate the previous displacement-based procedures to design base isolation protection devices, the Getty Villa located in Southern California, USA, which houses Greek and Roman artefacts in its open spaces, is considered. For that site, a design response spectrum according to the ASCE Standard[66] is derived using the following parameters[67]: (a) site-adjusted short period (0.2 s) spectral acceleration $S_{DS} = 14.61$ m/s^2; (b) site-adjusted one-second period (1.0 s) spectral acceleration $S_{D1} = 6.57$ m/s^2; and (c) transition period between constant spectral velocity and constant spectral displacement ranges of the spectrum of $T_L = 8.0$ s. A rubber bearing isolator with a 5% damping ratio is assumed. However, in the last section of the paper two additional design examples are presented, which consider larger damping ratios. In the following analyses, the mass ratio is assumed to be constant for all simulations and equal to $\gamma_b = 0.9$. Additionally, the density of the block remains constant, implying that the mass of the isolator always accounts for approximately 10% of the total system mass. To validate the procedure, a suite of accelerograms was used; 11 spectrum-compatible records (Figure 7) were selected using the software incorporated in the Pacific Earthquake Engineering Research Center database.[68] The software uses the mean squared error (MSE) to assess the match between a time series and a target spectrum. The MSE is determined by comparing the spectral accelerations of the recorded data with those of the target spectrum, within an assigned period range (in this case, 0.1 to 10 s). Additionally, the MSE is divided by a weight function, denoted as $w(T_i)$, which is used to assign relative weights to different parts of the period range. The weight function is discretized at each period T_i, where the MSE is calculated. In the case at hand only unity weights were assumed, hence the MSE is not modified. Additional information on the software for selecting earthquake ground motion time histories can be found in.[69] Further, the selection of records was confined to a specific range of moment magnitudes, between 6.5 to 7.5, as well as a range of average shear velocities in the top 30 m, spanning from 360 to 760 m/s. The following subsections report parametric analyses that show and validate the proposed design procedures.

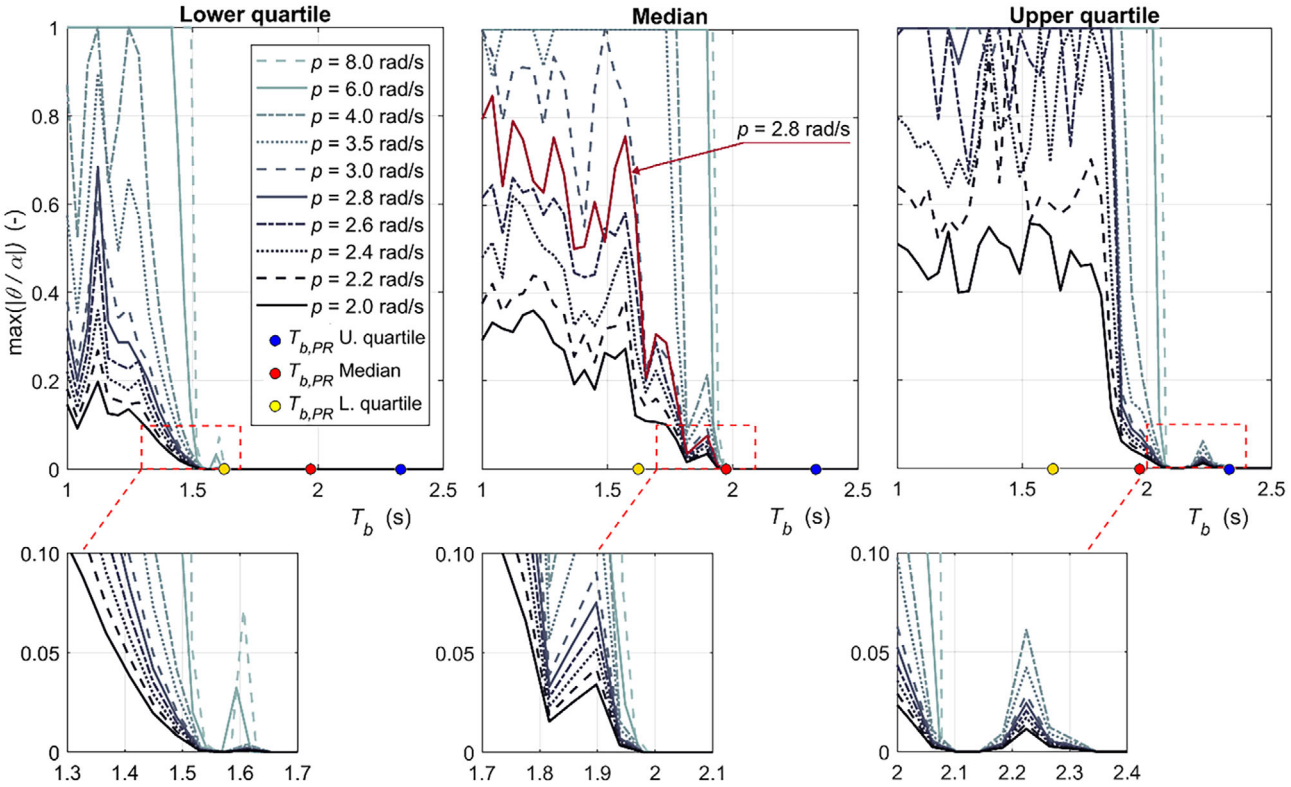

FIGURE 8 Lower quartile, median and upper quartile for the accelerograms suite in Figure 7A and in Table A1, of the maximum absolute nondimensional rotations for rigid blocks, varying the frequency parameter p and the period of the isolator T_b. $\alpha = 0.3$ rad.

4.1 | PRDBD method

The PRDBD method is used to design base isolation devices in order to prevent the rocking motion of the upper block. In the following analyses, a block slenderness angle $\alpha = 0.30$ rad is assumed to validate the procedure. This angle involves a minimum uplift acceleration of 2.95 m/s^2, and the minimum period of the isolator that prevents rocking motion is thus $T_{b,PR} = 2.20$ s (from now called the "minimum isolator period"). The previous period is calculated using Equation (5), in which the target displacement d_t in the ADRS plane is assumed as the intersection of the minimum uplift acceleration and the design spectrum. This calculation delivers a value of $d_t = 0.37$ m, as shown in Figure 7B.

Several time history analyses are carried out for various block sizes using the suite of records in Figure 7A and Table A1. The upper quartile, median, and lower quartile of the maximum absolute nondimensional rotations for the rigid block are evaluated for the suite of accelerograms while varying the period of the base isolation between 1.00 and 2.50 s (Figure 8). To understand the effect of the block size, a realistic range of frequency parameters (a measure of the dynamic characteristics of the rigid block) is investigated (Figure 8): from $p = 2$ rad/s (i.e., a large electric transformer) to $p = 8$ rad/s (i.e., a household brick). According to the PRDBD procedure, rocking motion cannot be triggered if an isolator with a period equal or lower than $T_{b,PR}$ (calculated analytically) is used. To validate the procedure, the period of the isolator calculated using the PRDBD procedure is compared with the smallest isolator period (among investigated frequency parameter p values) obtained from the median response (over the bin of 11 records) of the time history analysis (Figure 8), for which rocking motion is prevented. The median response of the numerical analysis shows that to prevent rocking motion the period of the isolator should exceed 1.95 s (red dots in Figure 8), while according to the PRDBD procedure $T_{b,PR} = 2.20$ s. The difference between these two values is small and is on the safe side for the equivalent static procedure. The median response also reveals that the size of the block does not influence the minimum isolator period, as expected. Further, the upper quartile response shows that even for the records that happen to generate a larger response near the analytically obtained value of $T_{b,PR} = 2.20$ s, the rocking response is still very minimal up to $T_b = 2.35$ s (blue dots in Figure 8), and no rocking occurs for longer periods. Meanwhile, the lower quartile response shows that rocking motion is prevented for an isolator period below approximately 1.65 s (yellow dots in Figure 8).

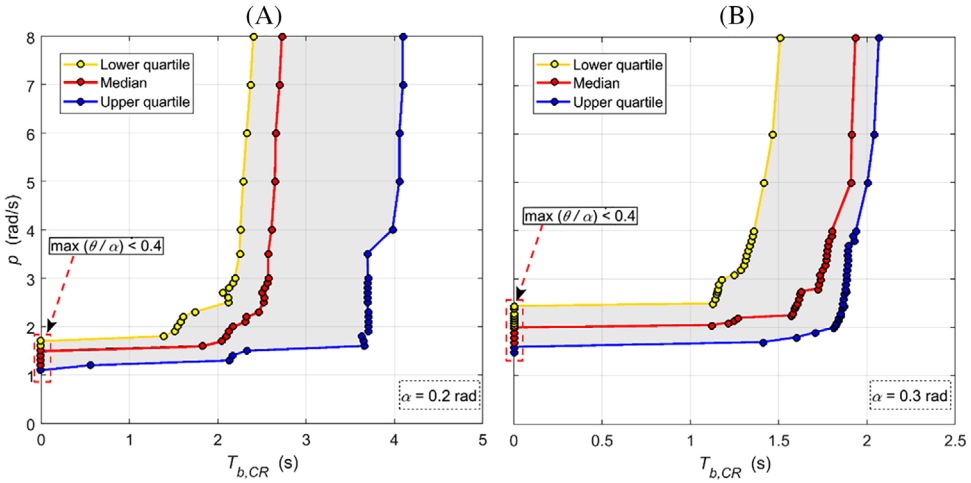

FIGURE 9 Median, upper and lower quartiles, for the suite of accelerograms in Table A1, of the isolator period $T_{b,CR}$ (for which the maximum rotation is approximately 40% of the maximum rotation capacity), varying the size (hence its frequency parameter p) and the slenderness (hence its slenderness angle α) of the block: (A) $\alpha = 0.2$; (B) $\alpha = 0.3$ rad.

Although it is not in the scope of the PRDBD procedure, it is possible to make interesting observations by examining the response of the system for isolator periods shorter than the numerical minimum isolator period, that is, when rocking motion is initiated (Figure 8). In this case, increasing the size of the block (smaller p), the rotation decreases. This observation confirms the well-known scale effect pointed out by Housner.[1] As a result, for larger blocks isolators with periods smaller than $T_{b,PR}$ may result in rotations that may be acceptable, while for small blocks, overturning may occur for isolators with periods relatively close to $T_{b,PR}$.This indicates that for small objects, the prevented rocking approach should be pursued.

In conclusion, the validation study demonstrated that the PRDBD procedure is generally applicable for designing base isolation devices to prevent the rocking motion of a rigid block. For the considered suite of accelerograms, the study revealed that (a) the method is particularly suitable for medium to small size objects with p greater than 2.8 rad/s (red curve in the median response of Figure 8); (b) for large size objects with $p \leq 2.8$ rad/s, the procedure may be too conservative, because rotations induced from the design earthquake may be acceptable. Indeed, for the median response, no overturning occurs for any period of the isolator for large blocks; (c) as the block size decreases (or the frequency parameter p increases) the transition from a nonrocking condition to overturning occurs for isolator period values getting closer to $T_{b,PR}$. For these cases the PRDBD procedure should be used with an adequate safety factor to avoid any rocking motion.

4.2 | CRDBD method

The CRDBD procedure is aimed at designing base isolation devices for rocking blocks, in order to allow a specified maximum rotation of the rigid block during the design earthquake. Here, as recommended by the commentary to the Italian building code,[64] this controlled rotation is expressed in terms of block center of mass displacement d_{CR}, assumed as 40% of the block maximum displacement capacity, d_0. The CRDBD procedure is based on the equal displacement rule, which must be validated for the seismically isolated rocking-block system. Multiple time history analyses using the suite of accelerograms in Table A1 are carried out for this purpose. The dynamic response of several blocks differing in size (hence having different frequency parameters p) is evaluated for two slenderness angle values: (a) $\alpha = 0.20$ rad (Figure 9A); (b) $\alpha = 0.30$ rad (Figure 9B). The analysis is carried out for each block by varying the period of the isolator until the maximum absolute displacement of the block over the suite of accelerograms approximately equals d_{CR}. The corresponding period of the isolator is called the numerical controlled rocking period. Then the median, upper, and lower quartiles of the response varying block size and slenderness angle are calculated (Figure 9). The median response of the blocks with slenderness angle $\alpha = 0.30$ rad (Figure 9B) shows that for large blocks ($p < 2$ rad/s) the numerical controlled rocking period tends to zero (i.e., the dots on the left edge of the inset figure). This behavior indicates that the system does not exceed the displacement limit imposed by the CRDBD procedure for any period of the isolator, so no isolator is required. As the size of the block decreases (thus increasing p), the numerical controlled rocking period increases, approaching the isolator

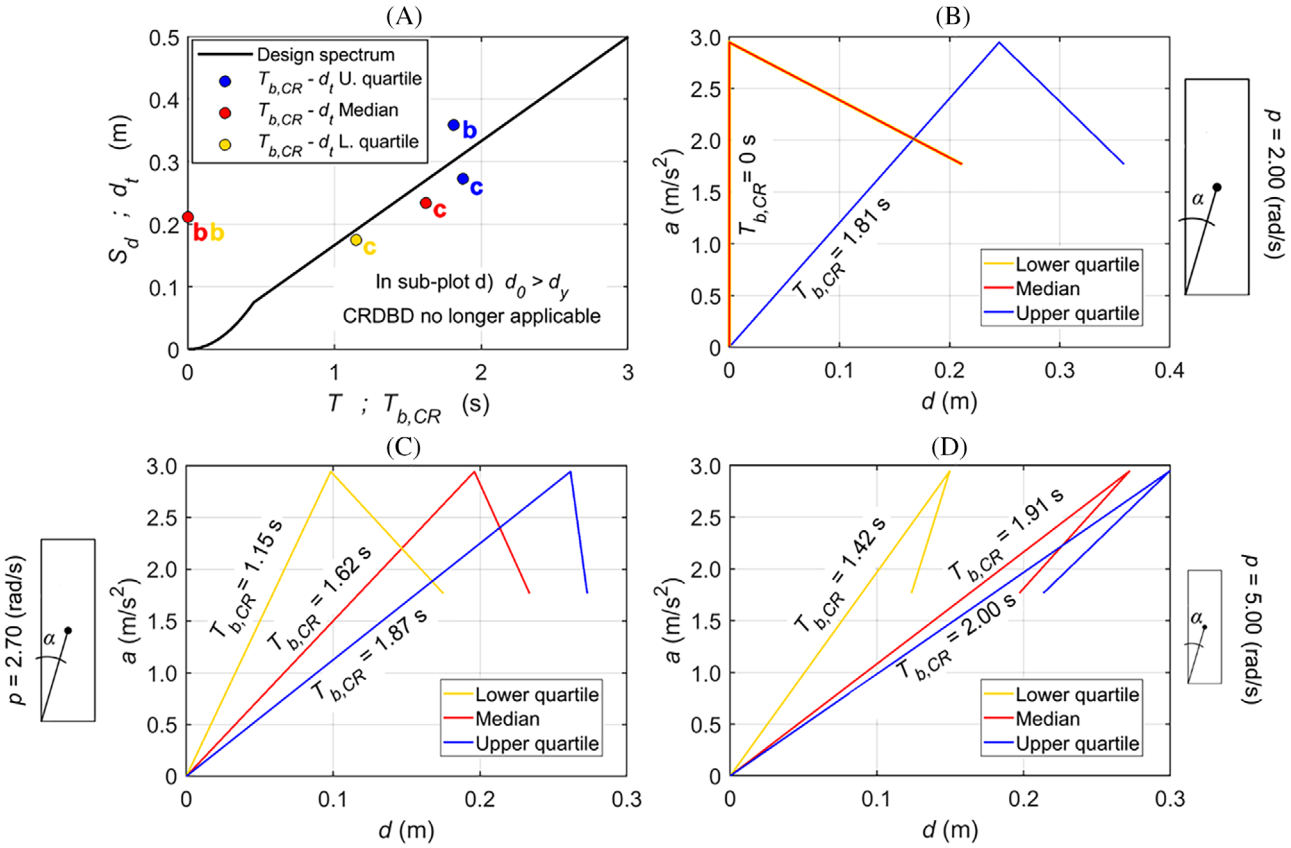

FIGURE 10 (A) Comparison, in the displacement-period plane, between analytical displacement demand (design spectrum) and numerical results obtained from the capacity curves built using time history analysis for three cases: (B) $\alpha = 0.3$ rad and $p = 2.0$ rad/s; (C) $\alpha = 0.3$ rad and $p = 2.7$ rad/s; (D) $\alpha = 0.3$ rad and $p = 5.0$ rad/s.

period for which rocking motion is prevented (approximately 1.90 s). Similar observations can be made when assuming $\alpha = 0.20$ rad (Figure 9A). In this case, the numerical controlled rocking period tends to zero (i.e., the dots on the left edge of the inset figure) for larger blocks ($p < 1.5$ rad/s) than in the previous case. Again, as the size of the block decreases (i.e., p increases), the numerical controlled rocking period moves closer to the isolator period for which rocking motion is prevented. In this case, the block is more slender, resulting in a larger period (approximately 2.70 s). These results confirm that the CRDBD method strongly depends on the size of the block, as well as on its slenderness. Further, the relationship between $T_{b,CR}$ and p in terms of median, lower, and upper quartile response shows that the record-to-record sensitivity of the system changes as the slenderness of the rigid block increases (or the slenderness angle decreases).

Next, in order to validate the proposed CRDBD method, capacity curves are built (for blocks differing in size and slenderness) using the properties derived from the time history analysis. In particular, the first elastic branch of the capacity curve is obtained using the numerical controlled rocking period for which the maximum displacement of the block over the suite of accelerograms is d_{CR} (Figure 10A). The elastic branch is then extended up to the acceleration capacity $g \tan(\alpha)$, which is a function of the block slenderness. Next, the second branch exhibiting negative stiffness is added as described in the previous section and, finally, the target displacement is calculated as in Equation (6).

The validation process of the CRDBD method relies on the applicability of the equal displacement rule in the examined system, and to this purpose, the next steps are followed: (a) the median, lower and upper quartile responses (i.e., Figure 9) are used to derive the numerical controlled rocking period and the target displacement, for blocks with a range of sizes (i.e., p values); (b) the derived period and the characteristics (size and slenderness) of the corresponding block are used to build the capacity curve (as explained in the previous paragraph) and therefore to obtain the target displacement; (c) the design spectrum and the results are presented in the displacement-period plane (e.g., Figure 10A), where each dot represents a different p value and each color set represents a different quartile (lower, median, upper); (d) in order to validate the equal displacement rule, the displacement demand for the system is identified as the intersection between the vertical line passing through the period $T_{b,CR}$ (obtained numerically) and the design spectrum; (e) the effectiveness of

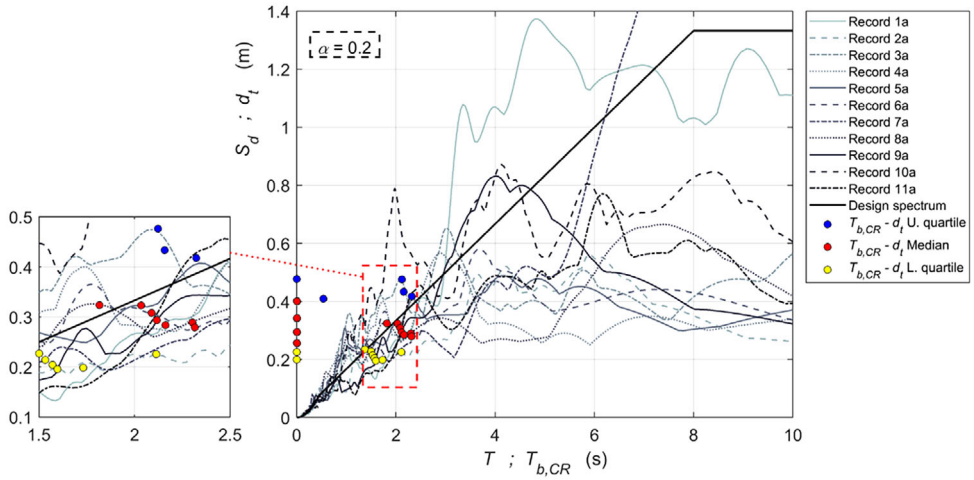

FIGURE 11 Comparison between analytical displacement demand (i.e., design spectrum) and capacity obtained numerically plotted in the displacement-period plane for blocks with $\alpha = 0.2$ rad and various sizes.

the CRDBD method can be graphically evaluated based on the difference between the target displacement d_t (obtained numerically) and the spectral displacement demand for the same period $T_{b,CR}$.

To clarify the validation procedure, three particular cases are examined in Figure 10. Assuming, for instance, a block with $R = 1.00$ m ($p = 2.7$ rad/s), and $\alpha = 0.3$ rad (Figure 10C), the numerical analysis shows that the (median) numerical controlled rocking period is $T_{b,CR} = 1.62$ s. In this case, the displacement capacity of the block is $d_{CR} = 0.12$ m and the elastic displacement of the isolator is $d_y = 0.20$ m, hence the target displacement is $d_t = 0.23$ m. Then, by applying the equal displacement rule, it is possible to determine the displacement demand as the point where the period of the isolator intersects with the design spectrum: for this case, the displacement demand is $S_{d,D} = 0.26$ m. Finally, to evaluate the effectiveness of the procedure, displacement demand and numerical capacity are compared. The results show a reasonable agreement between the two values (Figure 10C), providing a displacement demand slightly greater than the numerical capacity. When a larger block than the previous one is considered, with $R = 1.84$ m ($p = 2.0$ rad/s), it is possible to observe that the median numerical controlled rocking period of the isolator is equal to zero (Figure 10B): this value means that the maximum rotations (for any period of the isolator) do not overcome the assumed displacement capacity of the block. Further, if a small block with $R = 0.30$ m ($p = 5.0$ rad/s) is considered (Figure 10D), an additional scenario can be observed: the capacity curve exhibits a snapback behavior. As shown in the previous section, this snapback behavior happens when the isolator elastic displacement of the isolator at the uplift acceleration is larger than the displacement capacity of the block. In this case, the equal displacement rule is no longer applicable, hence the results are not included in the validation. Furthermore, for the case where $d_y < d_0$ and the CRDBD procedure is applicable (Figure 10C), if the upper quartile response is observed, it can be noticed that the contribution of the block displacement to the total displacement of the system decreases. On the other hand, when the lower quartile response is observed, the capacity of the block strongly contributes to the total displacement of the system. Hence, it can be stated that, when the displacement demand is small, the contribution of the allowed rocking to the global performance of the system becomes particularly important, reducing the demand on the isolator. Therefore, it can be affirmed that when the displacement demand is small, the contribution of the block controlled rocking towards enhancing the overall system performance becomes more appreciable. As a result, the burden on the isolator is reduced, meaning that the effectiveness of the CRDBD procedure increased. In this context, the effectiveness of the procedure refers to its ability to reduce demand in terms of period and damping ratio of the isolator, when compared to the characteristics required to prevent rocking motion.

Successively, the response was investigated for blocks with various sizes and $\alpha = 0.20$ rad. The results show generally a reasonable agreement between the median target displacements obtained numerically (red dots in Figure 11) and the analytical displacement demand (determined from the design spectrum). The method is particularly effective for medium to large size blocks, for which p ranges from 1.6 to 2.2 rad/s (Figure 11) and the corresponding numerical controlled rocking period ranges from 1.8 to 2.3 s. For blocks with $p > 2.3$ rad/s the capacity curves exhibit a snapback behavior. For these cases the CRDBD procedure is no longer applicable due to the unstable response of the system, as described in the previous section. Consequently, the results for these blocks are not included. For large blocks with $p < 1.5$ rad/s the numerical

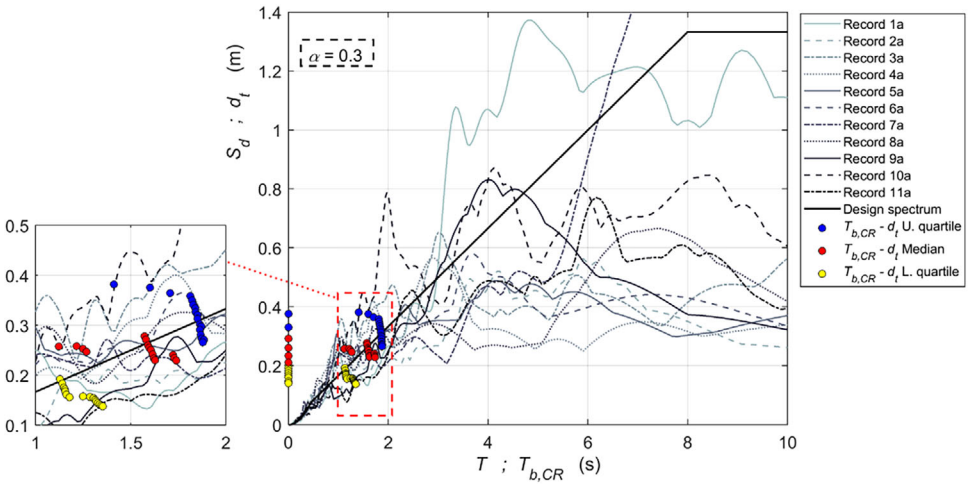

FIGURE 12 Comparison between analytical displacement demand (i.e., design spectrum) and capacity obtained numerically plotted in the displacement-period plane for blocks with $\alpha = 0.3$ rad and various sizes.

controlled rocking period tends to zero (hence, the dots on the left edge of Figure 11), indicating that the block does not exceed the 40% of the maximum rotation capacity imposed by the procedure for any period of the isolator. Consequently, it implies that no isolator is required. The upper and lower quartile responses (blue and yellow marks in Figure 11) are generally located above and below the design spectrum, respectively, as expected. The upper quartile response highlights the necessity of using isolators with a longer period than that of the median response in order to deliver the assumed controlled rotation for same block size. In this case, no isolator is required for blocks with $p < 1.2$ rad/s and the snapback behavior is observed for blocks with $p > 1.6$ rad/s. Conversely, the lower quartile response requires isolators with a period slightly shorter than that of the median response (for the same block size). In this case, the snapback behavior is observed for blocks with $p > 2.5$ rad/s while no isolator is required for blocks with $p < 1.8$ rad/s.

The validation procedure for $\alpha = 0.30$ rad (Figure 12) yields results similar to the previous case ($\alpha = 0.20$ rad). The median response (red dots in Figure 12) confirms the effectiveness of the procedure for medium-sized blocks, for which p ranges from 2.0 to 3.0 rad/s (Figure 11) and the corresponding numerical controlled rocking period ranges from 1.10 to 1.70 s. In this case, snapback behavior is observed for blocks with $p > 3.0$ rad/s while no isolator is required for blocks with $p < 2.0$ rad/s. The upper and lower quartile responses (blue and yellow marks in Figure 12) confirm the previous results (i.e., for $\alpha = 0.20$ rad), with an even smaller difference between the two responses. This finding was also observed in Figure 9, where a reduction in record-to-record variability for the upper quartile was observed for squatter blocks. The upper quartile response highlights that no isolator is required for blocks with $p < 1.7$ rad/s, while the capacity curves of the blocks with $p > 2.8$ rad/s exhibit snapback behavior. On the other hand, the lower quartile response pointed out that base isolation is not necessary for blocks with $p < 2.5$ rad/s and that blocks with $p > 4.0$ rad/s exhibit snapback behavior.

The CRDBD procedure has been found to be generally effective, and the main conclusions can be summarized as follows: (1) the equal displacement rule can be applied for isolating medium to large-size objects, that is, for blocks with $1.6 < p < 2.2$ rad/s and $\alpha = 0.20$ rad, as well as for blocks with $2.0 < p < 3.0$ rad/s and $\alpha = 0.30$ rad; (2) the applicability of the CRDBD method is limited for systems exhibiting a capacity curve with a snapback behavior; (3) the effectiveness of the CRDBD method increases for larger blocks because the contribution of the block displacement to the target displacement increases, allowing for the use of isolators with smaller periods (and therefore smaller isolator displacements) compared to the PRDBD method; (4) the procedure effectiveness increases for earthquakes with smaller displacement demand because the contribution of the block to the overall performance of the system increases.

5 | EXAMPLES AND DESIGN STRATEGIES

This section provides illustrations of two practical design examples, along with their respective validations, utilizing the PRDBD and CRDBD procedures for the seismic protection of real objects. The main purpose of these examples is to provide a pragmatic application of the proposed methods, highlighting their advantages and disadvantages in real scenarios.

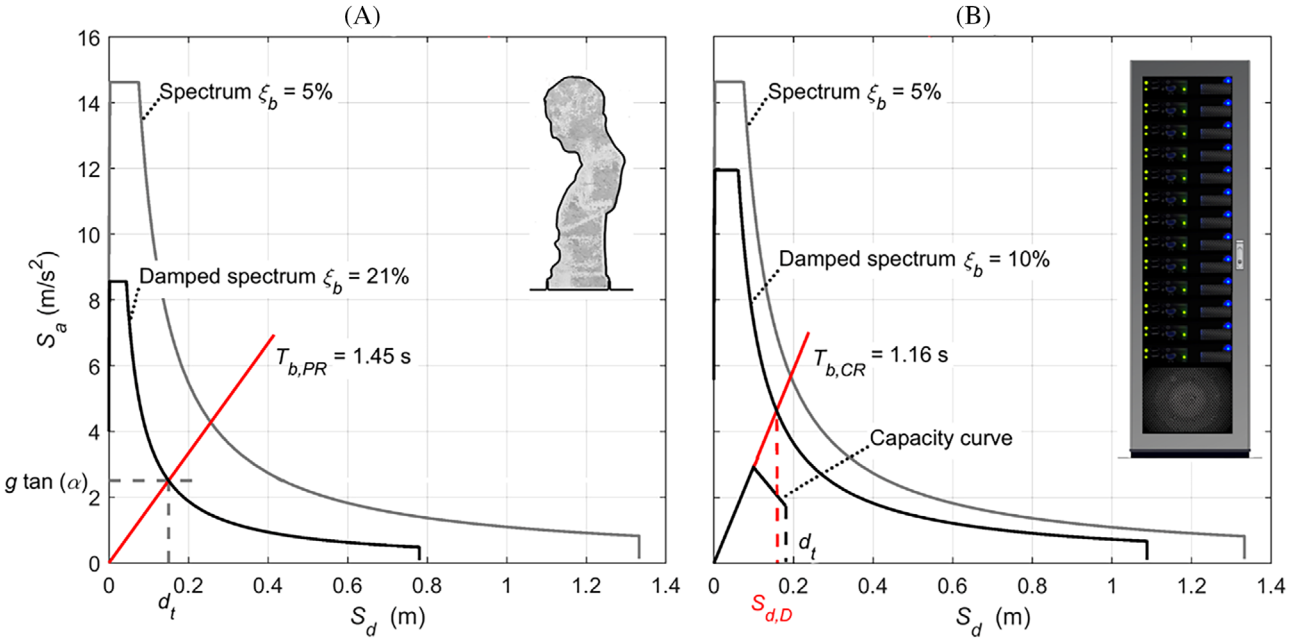

FIGURE 13 Design examples: (A) Isolator design for a Roman bust using the PRDBD method; (B) Isolator design for a computer server using the CRDBD method. CRDBD, controlled rocking displacement-based design; PRDBD, prevented rocking displacement-based design.

Finally, a protection strategy for objects, whose behavior can be modelled as rigid blocks when subjected to earthquakes, is presented. The strategy employs the proposed displacement-based methods and provides a rapid assessment to determine if protection strategies are necessary. The strategy emphasizes the use of base isolation technology for seismic protection.

5.1 | Example of PRDBD equivalent static design and nonlinear dynamic analysis

In this example, it is assumed that a Roman bust (Figure 13A) must be protected from earthquakes using base isolation technology. The real-life object is approximated as a rigid block with appropriate parameters ($2b = 0.22$ m and $2h = 0.75$ m; $p = 4.35$ rad/s). Considering that the object is fragile and extremely valuable, the isolator must be designed to avoid rocking motion, hence the PRDBD procedure must be used. Although the method has been described and validated for rectangular rigid blocks, this procedure can be applied with good safety level for a large variety of shapes, provided that the minimum uplift acceleration is known. In this example, the mass ratio is $\gamma_b = 0.9$, and the density of the block is 20 kN/m^3. The uplift acceleration is 2.88 m/s^2, while the target displacement is assumed to be $d_t = 0.15$ m. Therefore, the period of the isolator to prevent rocking motion is calculated as $T_{b,PR} = 1.45$ s. Finally, the code spectrum (Figure 7) must be scaled until $d_t = S_{d,D}$, in order to calculate the damping ratio of the isolator that prevents the uplift of the object. Various procedures are available in the literature to perform this task; however, the one proposed in the European code[70] is used here, in which the spectrum is scaled using the factor η:

$$\eta = \sqrt{\frac{10}{5 + \xi_b}}; \tag{7}$$

To prevent the initiation of rocking motion, the required damping of the isolator can be obtained by inverting the previous equation after calculating η as the ratio between the target displacement and the displacement demand. The values of η and ξ_b can be calculated as follows:

$$\eta = \frac{d_t}{S_{d,D}\left(T_{b,PR}\right)} \rightarrow \xi_b = \frac{10 - 5\eta^2}{\eta^2} = 21\% \tag{8}$$

Once the period and the equivalent damping of the isolator are calculated, the base isolation device can be designed. Then, to validate the analytical design procedure, time history analysis using a suite of spectrum-compatible accelerograms is required: Table A1 records are used in this case. Numerical analyses are performed with the center of mass of the isolator assumed as the control point for displacement. The results show an absolute maximum displacement of 0.12 m (median), 0.09 m (lower quartile), and 0.16 m (upper quartile). The numerical study demonstrates the validity of the method in terms of median maximum displacement, which is suitable since it is conservative. To validate the PRDBD procedure, it is also necessary to control the activation of rocking motion over the suite of records. In this case, it was observed that the median and lower quartile responses did not exhibit any rocking motion, while the upper quartile response showed that the block was overturned. This confirms that small blocks are more sensitive to input signals as highlighted previously. In light of these results, while the PRDBD procedure is efficacious in preventing rocking motion for the median response, it may be advisable to use a safety factor on the period of the isolator to further increase the protection level of the system. In this case, a safety factor of 1.50 was sufficient to prevent rocking for all earthquake records.

5.2 | Example of CRDBD equivalent static design and nonlinear dynamic analysis

A computer server (Figure 13B) must be protected because it is sited in a high seismicity area, such as the site previously studied. In this case, neglecting the effect of the containing structure, it is assumed acceptable the initiation of rocking motion during the code earthquake provided that the rotations do not exceed 40% of the maximum capacity. A typical 45 unit computer server rack has $2b = 0.60$ m and $2h = 2.00$ m ($p = 2.65$ rad/s), hence the slenderness angle of the system is $\alpha \approx 0.30$ rad. The displacement capacity (40% of the maximum capacity) is calculated as $d_{CR} = 0.12$ m. Once the capacity of the block has been determined, the isolator must be selected. In this case, the yield displacement is assumed $d_y = 0.10$ m ($< d_0$) and the damping $\xi_b = 10\%$. Therefore, the controlled rocking period of the isolator is $T_{b,CR} = 1.20$ s, and the target displacement is $d_t = 0.18$ m. After building the spectrum that accounts for the damping of the selected isolator, the spectral demand $S_{d,D}$ is calculated using the equal displacement rule as the intersection between the period $T_{b,CR}$ and the damped spectrum. Equation (9) indicates that the displacement demand is smaller than the target displacement, which means that the isolator is suitable for the required performance level.

$$d_t = 0.18 \text{ m};\ S_{d,D} = 0.16 \text{ m} \ \rightarrow d_t \geq S_{d,D} \tag{9}$$

Finally, the outcome of the analytical design procedure must be validated using time history analysis. To perform the numerical analysis for validation, it is necessary to define a set of spectrum-compatible accelerograms. In this case, the records of Table A1 are used, and the center of mass of the block is assumed as the reference point for displacement control. According to the numerical analysis conducted over the suite of records, the system exhibits a control point maximum displacements of 0.13 m (median), 0.10 m (lower quartile), and 0.16 m (upper quartile). Compared to the displacement demand, the median maximum displacement of the system is conservative. When using the CRDBD procedure, it is critical to check the maximum rotations of the rigid block, regardless of the displacement of the isolator. Based on the suite of accelerograms used in this study, the maximum rotation was found to be 41% (median), 13% (lower quartile), and 63% (upper quartile) of the maximum rotation capacity of the block. The median maximum rotation obtained from the numerical analysis aligns with the rotation capacity assumed during the design phase, however the results are slightly not conservative. To ensure a sufficient safety margin, an appropriate safety factor for the isolator period could be employed before finalizing the design. For example, suppose the designer desired the upper quartile rocking rotation to remain at 40% or below. For this example, a safety factor of 1.10 on the isolator period would be required.

To evaluate the difference between the CRDBD and PRDBD approaches, this second example was also designed using the PRDBD procedure. The resulting isolator had $\xi_b = 32\%$. Compared to CRDBD, the isolator requires a 220% increase in damping ratio. Further, assuming the same damping ratio as the previously selected isolator ($\xi_b = 10\%$), the inverted PRDBD procedure allows for calculating the period of the isolator (1.80 s) and the target displacement (0.25 m) required to prevent rocking motion. In this case, when compared to the CRDBD approach, the isolator designed using the PRDBD procedure required a 50% longer period and a 150% larger yield displacement of the isolator. From these comparisons, it becomes evident that the CRDBD approach offers several advantages over the PRDBD method, including a more efficient design with a smaller damping ratio (or shorter period and smaller total displacement) for the isolator.

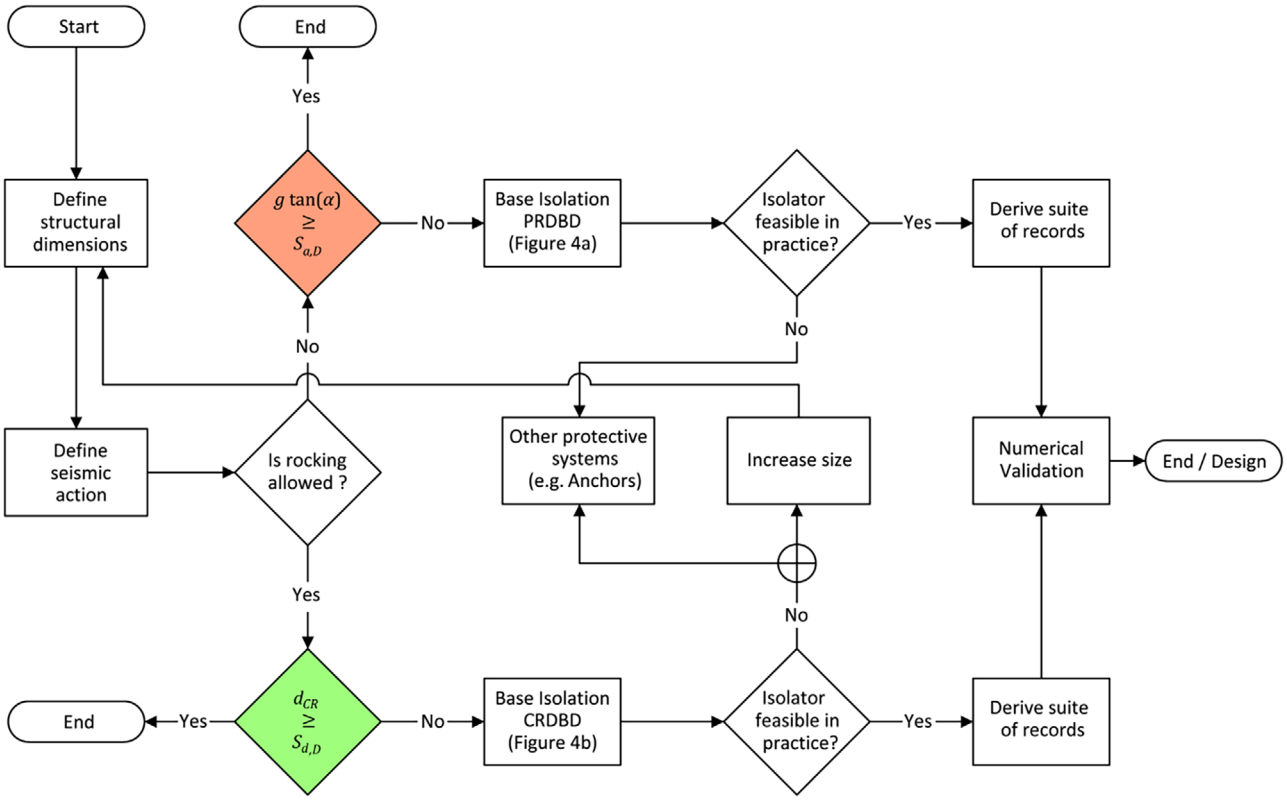

FIGURE 14 Seismic assessment and protection strategy flowchart.

5.3 | Seismic assessment and protection strategy procedure

This section proposes a procedure for seismic assessment of rigid blocks and for the potential design of the earthquake protection system, with a focus on base isolation. The flowchart for this procedure is shown in Figure 14, and the main steps are summarized below.

The first phase requires the definition of the geometry and capacity of the block, followed by the description of the seismic demand. Then, two options are possible (as shown in Figure 14): (a) rocking motion is not allowed; (b) rocking motion is allowed. To assess the seismic performance of the block (placed on a rigid foundation), the procedures provided by the commentary to the Italian building code[64] are used. Specifically, if rocking motion is not allowed, it is necessary to check if the uplift acceleration of the block is greater than the acceleration demand, $S_{a,D}$. If rocking motion is allowed, it is necessary to ensure that the displacement rocking capacity of the block is larger than the displacement demand, $S_{d,D}$, which is obtained according to the commentary to the Italian building code.[64] If the previous controls are not satisfied, seismic protection is required, and either PRDBD or CRDBD can be used, depending on whether rocking is allowed or not. After applying one of the two procedures, it must be checked if the device can be assembled using current technology (Figure 14). If this is not feasible, other protective systems such as anchoring devices can be used instead. Additionally, if CRDBD is used, an alternative option is to reduce the slenderness (e.g., by enlarging the base) or to increase the size (e.g., by adding a substantial pedestal) of the object and repeat the procedure. If the isolator is feasible in practice, a suite of spectrum-compatible records must be derived and used to validate the designed isolator using numerical simulations. This final step can be taken according to different codes and for different performances of the system.

6 | CONCLUSIONS

In this paper, two simplified methods to design base isolation devices for seismic protection of rocking rigid blocks are proposed. First, the analytical model of the system formed by a rocking block placed on a linear seismic isolation device is illustrated. Then, two procedures are introduced: (a) Prevented rocking displacement-based design (PRDBD); (b)

Controlled rocking displacement-based design (CRDBD). In the PRDBD procedure the isolator is designed to prevent the activation of rocking motion under the code earthquake. Conversely, the CRDBD procedure focuses on designing the isolator to allow a controlled rocking motion, enabling a specific maximum rotation of the block for the code ground motion. This method exploits the rotational capacity of the block to increase the overall performance of the system. The two procedures are successively validated by investigating the response of the system to a suite of accelerograms, thereby demonstrating the general effectiveness of the simplified methods.

The results for the PRDBD method reveal that the procedure is particularly efficacious for medium to small size objects ($p > 2.8$ rad/s). Furthermore, the analysis reveals a significant sensitivity of the system to the input signals. The analysis showed that the well-known scale effect pointed out by Housner[1] also applies to isolated rigid blocks. This result highlights that the PRDBD procedure is particularly suitable for small size objects where the transition from a nonrocking condition to overturning may occur suddenly.

The validation of the CRDBD procedure demonstrated its general applicability to seismically isolated rocking block systems, despite their negative stiffness. Moreover, this study found the equal displacement rule to be applicable for medium to large size blocks with $1.6 < p < 2.2$ rad/s and $\alpha = 0.20$ rad, as well as for blocks with $2.0 < p < 3.0$ rad/s and $\alpha = 0.30$ rad. However, for systems with a frequency parameter exceeding the upper limit of these ranges, capacity curves exhibiting a snapback behavior were observed. In such cases, rocking cannot be relied upon as a consistent behavior for design. The effectiveness of the CRDBD method increases with the size of the block, as its rotation significantly contributes to the overall performance of the system. This contribution becomes particularly evident when decreasing the earthquake displacement demand. Finally, practical design examples using the proposed procedure are illustrated and a simplified design of a protection strategy for these objects/structural elements is proposed.

Future studies might explore the impact of different base isolation devices on the proposed procedures. Additionally, alternative approaches, like the equal energy rule, could be investigated for the CRDBD method. Furthermore, research could be conducted to investigate the effect of different damping related spectra scaling procedures (e.g., use of conditional mean spectra) for this kind of systems. Finally, safety factors, obtained from a direct comparison between the procedures analytical results and numerical data, might be established based on fully probabilistic studies. Moreover, record-to record-variability of the system should be estimated as well, considering a large variety of record ground motions.

ACKNOWLEDGMENTS

This work was partially carried out under the MONALISA (MONitoraggio Attivo e Isolamento da vibrazioni e Sismi di oggetti d'Arte = Active monitoring and isolation from vibrations and earthquakes of art objects) research project funded by Lazio Regional Government and Italian Ministry of University and Research, project id. 305-2020-35576.

DATA AVAILABILITY STATEMENT

Data sharing not applicable to this article as no datasets were generated or analyzed during the current study.

ORCID

Giacomo Destro Bisol https://orcid.org/0000-0002-1266-9065
Matthew J. DeJong https://orcid.org/0000-0002-6195-839X
Luigi Sorrentino https://orcid.org/0000-0003-1652-942X

REFERENCES

1. Housner GW. The behavior of inverted pendulum structures during earthquakes. *Bull Seismol Soc Am*. 1963;53(2):403-417.
2. Yim C-S, Chopra AK, Penzien J. Rocking response of rigid blocks to earthquakes. *Earthq Eng Struct Dyn*. 1980;8(6):565-587.
3. Bao Y, Konstantinidis D. Dynamics of a sliding-rocking block considering impact with an adjacent wall. *Earthq Eng Struct Dyn*. 2020;49(5):498-523.
4. Elmorsy M, Vassiliou MF. Effect of ground motion processing and filtering on the response of rocking structures. *Earthq Eng Struct Dyn*. 2023;52(6):1704-1721.
5. Diamantopoulos S, Fragiadakis M. Modeling of rocking frames under seismic loading. *Earthq Eng Struct Dyn*. 2022;51(1):108-128.
6. Prajapati S, Destro Bisol G, Alshawa O, Sorrentino L. Non-linear dynamic model of a two-bodies vertical spanning wall elastically restrained at the top. *Earthq Eng Struct Dyn*. 2022;51(11):2627-2647.
7. Derakhshan H, Griffith MC, Ingham JM. Out-of-plane seismic response of vertically spanning URM walls connected to flexible diaphragms. *Earthq Eng Struct Dyn*. 2015;45(4):563-580.
8. Casapulla C, Giresini L, Lourenço PB. Rocking and kinematic approaches for rigid block analysis of masonry walls: state of the art and recent developments. *Buildings*. 2017;7(3):69.

9. Giresini L, Casapulla C, Denysiuk R, Matos J, Sassu M. Fragility curves for free and restrained rocking masonry façades in one-sided motion. *Eng Struct*. 2018;164:195-213.
10. Dar A, Konstantinidis D, El-Dakhakhni WW. Evaluation of ASCE 43-05 seismic design criteria for rocking objects in nuclear facilities. *J Struct Eng*. 2016;142(11):4016110.
11. Fragiadakis M, Diamantopoulos S. Fragility and risk assessment of freestanding building contents. *Earthq Eng Struct Dyn*. 2020;49(10):1028-1048.
12. Vlachakis G, Giouvanidis AI, Mehrotra A, Lourenço PB. Numerical block-based simulation of rocking structures using a novel universal viscous damping model. *J Eng Mech*. 2021;147(11):4021089.
13. Diamantopoulos S, Yanni H, Fragiadakis M, *Modeling of museum artifacts under seismic loading as two- block rocking systems*. 2022.
14. Sironi L, Andreini M, Colloca C, et al. Shaking table tests for seismic stability of stacked concrete blocks used for radiation shielding. *Eng Struct*. 2023;283:115895.
15. Derakhshan H, Walsh KQ, Ingham JM, Griffith MC, Thambiratnam DP. Seismic fragility assessment of nonstructural components in unreinforced clay brick masonry buildings. *Earthq Eng Struct Dyn*. 2020;49(3):285-300.
16. Huang B, Günay S, Lu W. Seismic assessment of freestanding ceramic vase with shaking table testing and performance-based earthquake engineering. *J Earthquake Eng*. 2022;26(15):7956-7978.
17. Berto L, Di Sarno L, Fragiadakis M, Rocca I, Saetta A. Seismic assessment of free-standing artifacts: full-scale tests on large shake table. *Earthq Eng Struct Dyn*. 2023;52:2708-2730.
18. Di Sarno L, Magliulo G, D'Angela D, Cosenza E. Experimental assessment of the seismic performance of hospital cabinets using shake table testing. *Earthq Eng Struct Dyn*. 2019;48(1):103-123.
19. Kuo K, Suzuki Y, Katsuragi S, Yao GC. Shake table tests on clutter levels of typical medicine shelves and contents subjected to earthquakes. *Earthq Eng Struct Dyn*. 2011;40(12):1367-1386.
20. Naeim F, Kelly JM. *Design of Seismic Isolated Structures: From Theory to Practice*. John Wiley & Sons; 1999.
21. Fenz DM, Constantinou MC. Behaviour of the double concave friction pendulum bearing. *Earthq Eng Struct Dyn*. 2006;35(11):1403-1424.
22. Roussis PC, Constantinou MC. Uplift-restraining friction pendulum seismic isolation system. *Earthq Eng Struct Dyn*. 2006;35(5):577-593.
23. Katsamakas AA, Vassiliou MF. Experimental parametric study and phenomenological modeling of a deformable rolling seismic isolator. *J Earthquake Eng*. 2023;27(16):4664-4693.
24. Giresini L, Puppio ML, Laccone F, Froli M. Experimental and numerical investigation on a passive control system for the mitigation of vibrations on SDOF and MDOF structures: mini Tribological ROCKing Seismic Isolation Device (miniTROCKSISD). *J Earthquake Eng*. 2022;26(14):7486-7504.
25. Podany J, eds. Advances in the Protection of Museum Collections from Earthquake Damage: Papers from a Symposium Held at the J. Paul Getty Museum at the Villa on May 3–4, 2006. Getty Publications; 2008.
26. Berto L, Favaretto T, Saetta A. Seismic risk mitigation technique for art objects: experimental evaluation and numerical modelling of double concave curved surface sliders. *Bull Earthquake Eng*. 2013;11(5):1817-1840.
27. Di Egidio A, Contento A. Base isolation of slide-rocking non-symmetric rigid blocks under impulsive and seismic excitations. *Eng Struct*. 2009;31(11):2723-2734.
28. Caliò I, Marletta M. Passive control of the seismic rocking response of art objects. *Eng Struct*. 2003;25(8):1009-1018.
29. Roussis PC, Pavlou E, Pisiara E, Base-isolation technology for earthquake protection of art objects. *Proceedings of the 14 th World Conference on Earthquake Engineering*;2008; Bejing. Innovation Practice Safety.
30. Roussis PC, Odysseos S. Rocking response of seismically-isolated rigid blocks under simple acceleration pulses and earthquake excitations. *Open Constr Build Technol J*. 2017;11(1):217-236.
31. Vassiliou MF, Makris N. Analysis of the rocking response of rigid blocks standing free on a seismically isolated base. *Earthq Eng Struct Dyn*. 2012;41(2):177-196.
32. Destro Bisol G, Dejong MJ, Liberatore D, Sorrentino L. Analysis of seismically-isolated two-block systems using a multi-rocking-body dynamic model. *Comput-Aided Civ Infrastruct Eng*. 2023;38:1583-1604. doi:10.1111/mice.13012
33. Pellecchia D, Lo Feudo S, Vaiana N, Dion J, Rosati L. A procedure to model and design elastomeric-based isolation systems for the seismic protection of rocking art objects. *Comput-Aided Civ Infrastruct Eng*. 2022;37(10):1298-1315.
34. Amarante dos Santos F, Fraternali F. Novel magnetic levitation systems for the vibration control of lightweight structures and artworks. *Struct Control Health Monit*. 2022;29(8):e2973.
35. De Canio G. Marble devices for the base isolation of the two bronzes of Riace: a proposal for the David of Michelangelo. *Proceedings of the 15th World Conference on Earthquake Engineering – WCEE*, Lisbon, Portugal, 24–28 September; 2012.
36. Di Egidio A, Contento A, De Leo AM, Gardoni P. Dynamic and seismic protection of rigid-block-like elements and structures on deformable ground with mass-damper dynamic absorbers. *J Eng Mech*. 2020;146(6):4020046.
37. Di Egidio A, Contento A, Olivieri C, de Leo AM. Protection from overturning of rigid block-like objects with linear quadratic regulator active control. *Struct Control Health Monit*. 2020;27(10):e2598.
38. Venanzi I, Ierimonti L, Materazzi AL. Active base isolation of museum artifacts under seismic excitation. *J Earthquake Eng*. 2020;24(3):506-527.
39. Cigada A, Zappa E, Paganoni S, Giani E. Protecting Pietà Rondanini against environmental vibrations with structural restoration works. *Int J Archit Heritage*. 2021;17(4):661-676.

40. Cui S, Bruneau M, Kasalanati A. Seismic response case study of isolated floor system having special biaxial spring units. *J Struct Eng*. 2016;142(12):1-13.
41. Cui S, Bruneau M, Kasalanati A. Behavior of bidirectional spring unit in isolated floor systems. *J Struct Eng*. 2010;136(8):944-952.
42. Wen J, Li X, Xie Q. Cost-effectiveness of base isolation for large transformers in areas of high seismic intensity. *Struct Infrastruct Eng*. 2022;18(6):745-759.
43. Lee D, Constantinou MC. Combined horizontal–vertical seismic isolation system for high-voltage–power transformers: development, testing and validation. *Bull Earthquake Eng*. 2018;16(9):4273-4296.
44. Lal KM, Whittaker AS, Constantinou MC. Mid-height seismic isolation of equipment in nuclear power plants. *Earthq Eng Struct Dyn*. 2023;52(4):998-1015.
45. Sato E, Furukawa S, Kakehi A, Nakashima M. Full-scale shaking table test for examination of safety and functionality of base-isolated medical facilities. *Earthq Eng Struct Dyn*. 2011;40(13):1435-1453.
46. Furukawa S, Sato E, Shi Y, Becker T, Nakashima M. Full-scale shaking table test of a base-isolated medical facility subjected to vertical motions. *Earthq Eng Struct Dyn*. 2013;42(13):1931-1949.
47. Priestley MJ, Calvi GM, Kowalsky MJ. Direct displacement-based seismic design of structures. In: *NZSEE Conference*; 30 March 2007:1-23.
48. Fardis MN, Panagiotakos TB. Displacement-based design of RC buildings: proposed approach and application. In: Fajfar P, eds. *Seismic Design Methodologies for the Next Generation of Codes*. 1st ed. Routledge; 1997:195-206.
49. Sullivan TJ, Priestley MJN, Calvi GM. Direct displacement-based design of frame-wall structures. *J Earthquake Eng*. 2006;10(1):91-124.
50. Cardone D, Palermo G, Dolce M. Direct displacement-based design of buildings with different seismic isolation systems. *J Earthquake Eng*. 2010;14(2):163-191.
51. Cardone D, Dolce M, Palermo G. Direct displacement-based design of seismically isolated bridges. *Bull Earthquake Eng*. 2009;7(2):391-410.
52. Ye K, Xiao Y, Hu L. A direct displacement-based design procedure for base-isolated building structures with lead rubber bearings (LRBs). *Eng Struct*. 2019;197:109402.
53. Priestley MJN, Evison RJ, Carr AJ. Seismic response of structures free to rock on their foundations. *Bull N Z Soc Earthq Eng*. 1978;11(3):141-150.
54. Makris N, Konstantinidis D. The rocking spectrum and the limitations of practical design methodologies. *Earthq Eng Struct Dyn*. 2003;32(2):265-289.
55. Nabeshima K, Taniguchi R, Kojima K, Takewaki I. Closed-form overturning limit of rigid block under critical near-fault ground motions. *Front Built Environ*. 2016;2:1-11.
56. Casapulla C, Jossa P, Maione A. Rocking motion of a masonry rigid block under seismic actions: a new strategy based on the progressive correction of the resonance response. *Ingegneria Sismica*. 2010;27(4):35-48.
57. Casapulla C. On the resonance conditions of rigid rocking blocks. *Int J Eng Technol*. 2015;7(2):760-771.
58. Reggiani Manzo N, Vassiliou MF. Displacement-based analysis and design of rocking structures. *Earthq Eng Struct Dyn*. 2019;48(14):1613-1629.
59. Reggiani Manzo N, Vassiliou MF. Simplified analysis of bilinear elastic systems exhibiting negative stiffness behavior. *Earthquake Eng Struct Dyn*. 2021;50(2):580-600.
60. Sorrentino L, Masiani R, Griffith MC. The vertical spanning strip wall as a coupled rocking rigid body assembly. *Struct Eng Mech*. 2008;29(4):433-453.
61. Lucchini A, Franchin P, Mollaioli F. Uniform hazard floor acceleration spectra for linear structures. *Earthq Eng Struct Dyn*. 2017;46(7):1121-1140.
62. Degli Abbati S, Cattari S, Lagomarsino S. Theoretically-based and practice-oriented formulations for the floor spectra evaluation. *Earthq Struct*. 2018;15(5):565-581.
63. Higashino M, Okamoto S. *Response Control and Seismic Isolation of Buildings*. Taylor and Francis; 2006.
64. Circolare Ministeriale del 21/01/2019 n.7, 2019 – Istruzioni per l'applicazione dell'«Aggiornamento delle "Norme tecniche per le costruzioni"». 2019. [in Italian].
65. Bommer JJ, Mendis R. Scaling of spectral displacement ordinates with damping ratios. *Earthq Eng Struct Dyn*. 2005;34(2):145-165.
66. ASCE STANDARD. *41-17 Seismic Evaluation and Retrofit of Existing Buildings*. 2017.
67. McKenzie L, Farrar B, Armendariz D, Podany J. Protecting collections in the J. Paul Getty museum from earthquake damage. *WAAC Newsletter*. 2007;29(3):16-23.
68. PEER ground motion database. *PEER NGA-West2 Database* 2013.
69. Wang G, Youngs R, Power M, Li Z. Design ground motion library: an interactive tool for selecting earthquake ground motions. *Earthquake Spectra*. 2015;31(2):617-635.
70. CEN. Eurocode 8 - Design of structures for earthquake resistance - Part 3: Assessment and retrofitting of buildings. EN 1998–3:2005, Brussels; 2005.

How to cite this article: Destro Bisol G, DeJong MJ, Liberatore D, Sorrentino L. Displacement-based design procedures for rigid block isolation. *Earthquake Engng Struct Dyn*. 2024;53:1552–1572. https://doi.org/10.1002/eqe.4074

APPENDIX A

TABLE A1 Spectrum compatible records.

ID	Earthquake name	Year (-)	M_w [a] (-)	Station name	V_{S30} [b] (m/s)	Record	SF [c] (-)
1a	San Fernando, CA, USA	1971	6.61	Santa Felita Dam	389	FSD172	5.95
2a	Imperial Valley, CA, USA	1979	6.53	Cerro Prieto	472	CPE147	3.72
3a	Irpinia, Italy	1980	6.90	Calitri	456	CTR000	3.50
4a	Corinth, Greece	1981	6.60	Corinth	361	COR-L	2.72
5a	Loma Prieta, CA, USA	1989	6.93	Coyote Lake Dam—Southwest Abutment	561	CYC195	3.72
6a	Northridge, CA, USA	1994	6.69	Sunland—Mt Gleason Ave	402	GLE170	4.32
7a	Duzce, Turkey	1999	7.14	Lamont 1061	481	1061-N	6.52
8a	Manjil, Iran	1990	7.37	Abbar	724	ABBAR-L	1.43
9a	Landers, CA, USA	1992	7.28	North Palm Springs Fire Sta. #36	368	NPF090	3.98
10a	Chuetsu-oki, Japan	2007	6.80	Joetsu Yasuzukaku Yasuzuka	655	65004NS	3.81
11a	Iwate, Japan	2008	6.90	Kurihara City	512	48A61NS	1.26

[a] M_w = Moment magnitude.
[b] V_{S30} = Average shear wave velocity of top 30 m of the site.
[c] SF = Scale factor.